Ultramicroscopy 110 (2010) 599–604

Contents lists available at ScienceDirect

Ultramicroscopy

journal homepage: www.elsevier.com/locate/ultramic

MEMS-based fast scanning probe microscopes

F.C. Tabak [a,*], E.C.M. Disseldorp [a], G.H. Wortel [a], A.J. Katan [b], M.B.S. Hesselberth [a], T.H. Oosterkamp [a], J.W.M. Frenken [a], W.M. van Spengen [a,c]

[a] Leiden University, Niels Bohrweg 2, 2333 CA Leiden, The Netherlands
[b] Lawrence Berkeley National Laboratory, 1 Cyclotron Road, Berkeley, CA, USA
[c] Falco Systems, Gelderlandplein 75L, 1082 LV Amsterdam, The Netherlands

ARTICLE INFO

Keywords:
MEMS
Scanning probe microscopy
High-speed scanning

ABSTRACT

Scanning probe microscopy is a frequently used nanometer-scale surface investigation technique. Unfortunately, its applicability is limited by the relatively low image acquisition speed, typically seconds to minutes per image. Higher imaging speeds are desirable for rapid inspection of samples and for the study of a range of dynamic surface processes, such as catalysis and crystal growth. We have designed a new high-speed scanning probe microscope (SPM) based on micro-electro mechanical systems (MEMS). MEMS are small, typically micrometer size devices that can be designed to perform the scanning motion required in an SPM system. These devices can be optimized to have high resonance frequencies (up to the MHz range) and have very low mass (10^{-11} kg). Therefore, MEMS can perform fast scanning motion without exciting resonances in the mechanical loop of the SPM, and hence scan the surface without causing the image distortion from which conventional piezo scanners suffer. We have designed a MEMS *z*-scanner which we have integrated in commercial AFM (atomic force microscope) and STM (scanning tunneling microscope) setups. We show the first successful AFM experiments.

1. Fast scanning probe microscopy

The scanning probe microscope is a very important instrument in surface science. It provides atomic resolution on a wide range of surfaces and is used to study processes from materials growth to biological binding events. SPMs can be designed to enable imaging under difficult circumstances: cryogenic temperatures, high pressures, in liquids, etc. [1–3]. Fast scanning is desirable for the study of fast surface processes: e.g. catalytic processes, biological processes and materials growth.

An example of a catalytic process that one might study with an SPM is the reaction $C_2H_4+3O_2 \rightarrow 2CO_2+2H_2O$, which takes place in a fuel cell on a platinum catalyst. It has been reported [4] that the reaction rate is 3.6 reactions per second per surface Pt atom. To properly study this, an imaging rate of at least 10 frames/s would be needed.

An example of a biological process is the binding of DNA to the streptavidin protein, which happens in approximately 0.4 s [5]. In order to acquire 10 images during a single binding event, an imaging rate of 25 images/s is required.

The growth of a thin film is a complex dynamical process. To exercise control over film uniformity a high level of understanding of detailed atomic mechanisms such as atomic hopping and diffusion across or over steps is required [6]. Dong et al. [7] report growing a ZnO thin film at 0.1 nm/s. This means that the growth of one single atom layer takes approximately 5 s, which would necessitate a frame rate of at least 1 frame/s; since this process is not uniform over the surface, a higher imaging rate would be desirable.

Unfortunately, an SPM is a relatively slow instrument. The acquisition of a single image typically takes several seconds to minutes. The scan speed is usually limited by two factors. The first is the fundamental resonance frequency of the scanning element (usually a piezo element). Typical resonance frequencies for piezo tubes are tens of kHz and for piezo stacks with additional damping mechanisms, the current state-of-the-art is 540 kHz [8]. The driving signals that move the piezo element over the surface should not have components with frequencies above the fundamental resonance frequency of the piezo element. Attempting to drive the piezo element at or above its resonance frequency will result in an unstable feedback loop and oscillations. Secondly, the motion of the piezo element can excite resonances in the mechanical loop of the scanning probe microscope as a whole. As the resolution is very high (10^{-10} m), any vibration will lower the image quality significantly. Small-amplitude vibrations may

* Corresponding author.
E-mail address: tabak@physics.leidenuniv.nl (F.C. Tabak).

0304-3991/$ - see front matter © 2010 Elsevier B.V. All rights reserved.
doi:10.1016/j.ultramic.2010.02.018

cause loss of the atomic resolution, while larger excursions may lead to tip crashes which can cause severe damage to both sample and tip.

Despite these limitations, high scan speeds have been obtained already with piezo-based scanners [8–12]. Even scan speeds up to 1000 images/s have been obtained [13] albeit for scanning without feedback. Impressive as this may be, the lack of feedback disqualifies the fast SPM for most of the desirable, high-speed applications mentioned above.

2. MEMS-based SPM

Micro-electro mechanical systems (MEMS) are devices with micrometer-sized features which perform electronic and mechanical actions. These devices can be designed to perform SPM-like motion and MEMS SPM devices have been designed previously by a number of groups [14–17]. The development of miniature cantilevers aside, these efforts have not led to a wide use of MEMS SPM scanners to date. The dimensions of these MEMS scanners are typically 100 μm wide, hundreds of micrometers to a millimetre long and tens of micrometers thick. These dimensions are not small enough to allow high resonance frequencies.

Part of MEMS SPM design has concentrated on high-density data storage applications, the most famous example being the IBM Millipede [18,19]. None of these designs has made it to commercial applications yet. A significant weakness is the write/read speed of these devices; an optimized MEMS might read/write at a rate of a Mbyte/s, while modern hard drives read/write at a Gbyte/s [20].

To our knowledge, no other recent MEMS SPM project has been focusing on high-speed scanning. We propose that MEMS scanners can be designed to be used as ultra high-speed scanners, which is explained below. In addition, we emphasize that when used as a 'regular' AFM or STM, a MEMS SPM does not have a significant advantage over a piezo-based SPM. MEMS are difficult to handle due to their small size and are very sensitive to the environment (dust, liquid). Furthermore, MEMS are not suitable as a general-purpose sample stage since this would impose stringent limits to the sample size and weight. Using the MEMS as a tip holder implies that a tip has to be integrated on the MEMS; the tip should either be fabricated during the growth process or deposited on the MEMS afterwards.

Despite these restrictions and difficulties, MEMS scanners beat piezo configurations when it comes to resonance frequencies. Already in the first generation of our designs, we have made working scanners with resonance frequencies up to 1.5 MHz. This is almost a factor three above the current best effort in piezo scanners. Thus, MEMS scanners can be actuated at unprecedented speeds. Of course, the mechanical loop should not be influenced by this high-speed motion. In a piezo scanner the mechanical loop would have to be designed extremely stiff. In MEMS scanners, however, this is not a problem since the weight of the MEMS is very small (typically 10^{-11} kg) so it will not influence the mechanical loop of the scanner (a problem that is apparent in piezo-based scanners, as described above). This means that the MEMS scanner can be actuated at high speeds while the other parts of the scanner will not move. In theory, the mechanical loop could be designed with an extremely low resonance frequency and still it would not be influenced by the motion of the MEMS scanner.

Ultimately, a scanner would be required with very high resonance frequencies in all three directions, i.e. *x*, *y* and *z*. However, combining high resonance frequencies in all directions is not straightforward. Therefore, we first focus on designing a uniaxial scanner with a high resonance frequency in the most demanding direction, the *z*-direction in which a feedback signal is used to keep the tip–sample separation constant. For this purpose, an AFM cantilever might appear as the obvious configuration. However, typical AFM cantilevers have relatively low resonance frequencies.

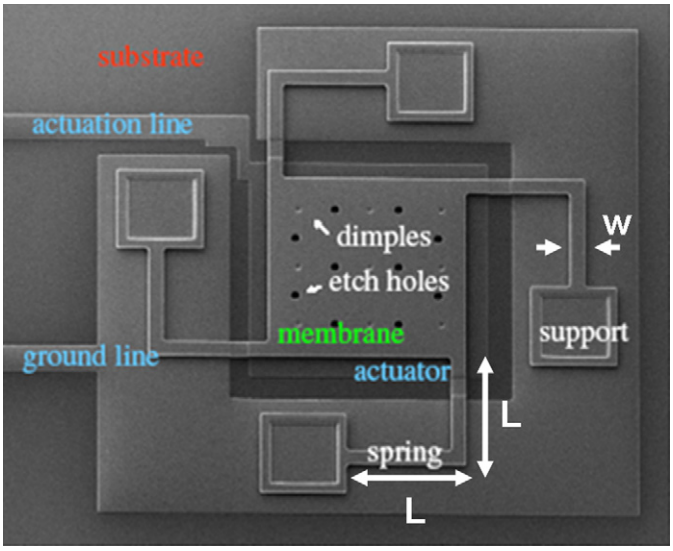

Fig. 1. The Leiden MEMS SPM. The SPM consists of a scanning plate (the membrane), which is supported by four springs. These springs are connected to four supports, which are fixed to the substrate and the ground line. The membrane is suspended 2 μm above the actuator plate. This actuator plate is connected to the outside world by the actuator line.

We have designed a MEMS SPM *z*-scanner, which is shown in Fig. 1. The scanner consists of a scan plate which is suspended by four springs, fixed on supports. The scan plate is suspended 2 μm above an actuation plate. Depending on the dimensions of the scan plate and the springs, the MEMS SPM scanner can have a fundamental resonance frequency up to 1.5 MHz. This is a *z*-scanner only and it needs to be integrated with a separate *x*,*y*-scanner. The scan plate is actuated by electrostatic forces, as explained below, with voltages in the range from 10 to 150 V.

MEMS SPM structures have been produced according to our designs at MEMSCAP [21], a company that offers a commercial MEMS production process in which each run is shared by multiple users. Of course, when using a multi-user MEMS fabrication process, one is limited to the design rules of this process, although one can add process steps on individual dies after the production has been completed. Good MEMS scanners have been obtained from the MEMSCAP PolyMUMPS (Multi-User MEMS Process) process.

3. MEMS resonance frequencies vs. scan range

In MEMS, as in piezo scanners, there is a trade-off between resonance frequency and scan range. Our uniaxial MEMS *z*-scanners have fundamental resonance frequencies up to 1.5 MHz (depending on the geometry), while maintaining a scan range in the *z*-direction of approximately 200 nm. This range is just sufficient for STM experiments. For MEMS with resonance frequencies between 250 kHz and 1.5 MHz, the scan range varies between 850 and 200 nm. For multi-axis MEMS structures, i.e. *x*,*z* – and *x*,*y*,*z*-scanners, it is extremely difficult to obtain a reasonable scan range of 200 nm or more while maintaining a high resonance frequency in all directions. Therefore, we believe that the most promising application lies in MEMS *z*-scanners integrated in fast piezo-based *x*–*y* scanners.

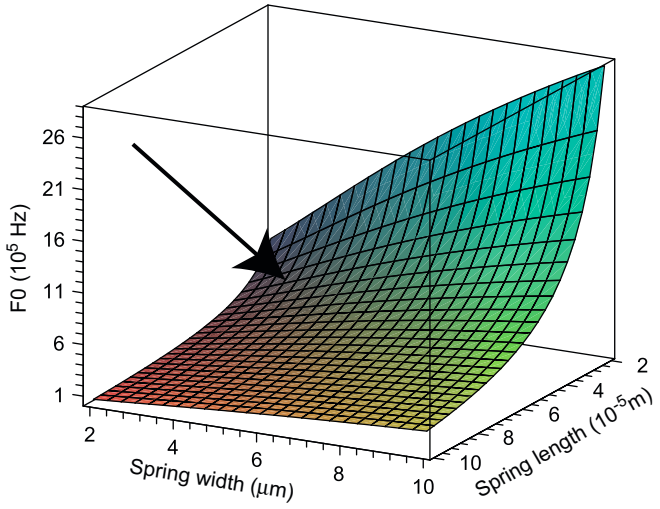

Fig. 2. Fundamental resonance frequency vs. geometrical properties, calculated analytically for a crab-like MEMS device, by use of Eq. 1. The thickness of the device is fixed to 2 μm, and the membrane is 40 μm × 40 μm. The length l and width w of the legs are variables expressed in meter. The resonance frequency is plotted on the z-axis in Hz. The geometry of our MEMS scanner ($l = 20$ μm, $w = 2$ μm) is indicated by the arrow.

The fundamental resonance frequency of a structure is determined by its spring constant k and its mass m by the relationship $f_0=(1/2\pi)^*\sqrt{(k/m)}$. The spring constant and mass are, in turn, determined by the geometrical properties and the material properties like Young's modulus and the Poisson ratio.

For a crab-leg flexure device, such as our SPM the spring constant is given by [22]

$$k=\frac{2Ew(t/l)^3}{2+6[1+\nu]/[1+(w/t)^2]} \quad (1)$$

Here, E is Young's modulus, w the width of the legs, t their thickness and l their length; ν is Poisson's ratio. This formula is valid only for crab-like flexure structures with equally long legs, as is the case in all of our MEMS scanners.

We control the z-motion by electrostatic actuation of the MEMS scanner. Applying a voltage difference V between a membrane and an actuation electrode results in a force on the membrane given by

$$F=-\frac{1}{2}\frac{\varepsilon_0 AV^2}{d^2}=-kx \quad (2)$$

A is the surface overlap between actuation electrode and membrane and d their separation. The second part of the equation indicates that the elastic counterforce satisfies Hooke's law (for small displacements of the membrane). Combining (1) and (2), we find the displacement of the membrane as a function of applied voltage and geometrical properties of the scanner. In Fig. 2 we show the relationship between the fundamental resonance frequency and geometrical properties and in Fig. 3 the relationship between displacement as a function of geometrical properties, for an actuation voltage of 100 V. The geometry of our MEMS scanner is indicated in the figures.

To optimise our MEMS design process and to acquire additional information about the deformation of the MEMS scanner during actuation and the deformation patterns, we have modelled the new MEMS structures with the COMSOL finite-element analysis package [23]. In this way, we can model both the actuation properties and the resonance frequencies of our devices. An example of a MEMS actuation simulation is shown in Fig. 4 for a scanner with a membrane of 40 μm × 40 μm and legs of 40 μm length, 2 μm thickness and 4 μm width. We have simulated

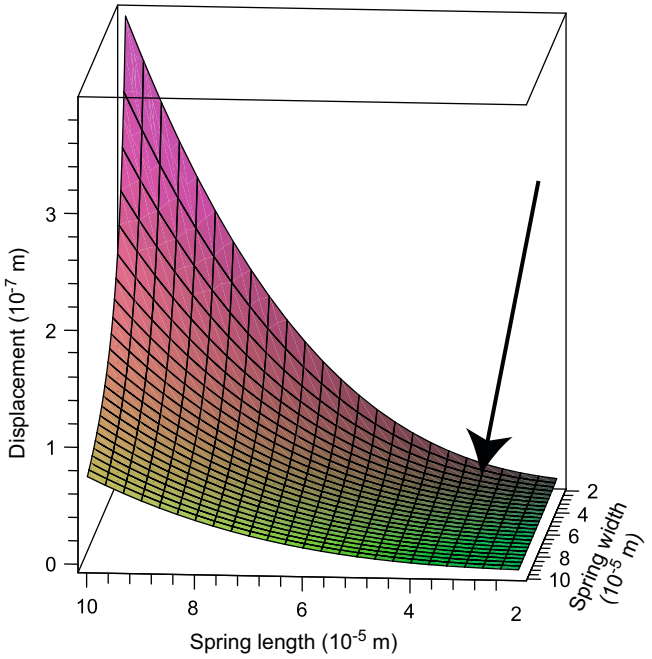

Fig. 3. Membrane displacement at an actuation voltage of 100 V as a function of geometrical properties, calculated analytically for a crab-like MEMS device, using Eqs. (1) and (2). The thickness of the device is fixed to 2 μm, and the membrane is 40 μm × 40 μm. The length l and width w of the legs are variables expressed in meter. The displacement is plotted on the z-axis in m. The geometry of our MEMS scanner ($l = 20$ μm, $w = 2$ μm) is indicated by the arrow.

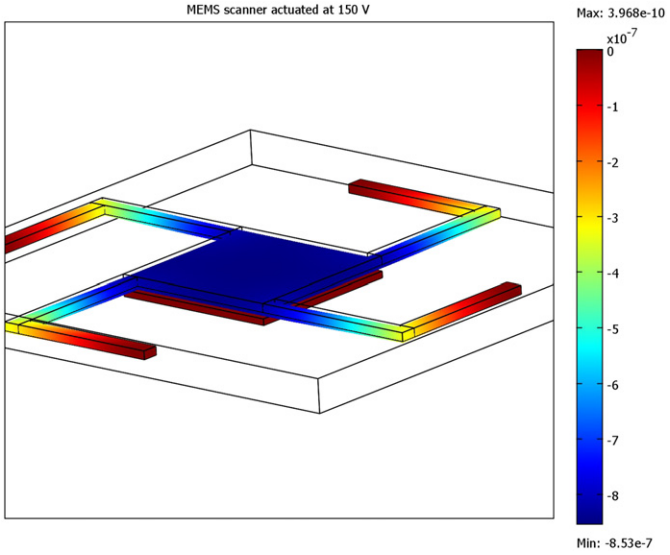

Fig. 4. Static deformations of a MEMS scanner with a 40 μm × 40 μm membrane, 40 μm legs with a width of 4 μm, without actuation (thin lines) and with 150 V actuation (solid model). Between 0 and 150 V this structure moves over 850 nm. The deformations have been obtained from finite-element calculations, as explained in the text.

MEMS actuation at both 50 and 150 V and we see that, when we use 150 V as maximum actuation voltage, we have a scan range of 850 nm. This MEMS has a fundamental resonance frequency of 261 kHz (Fig. 5). If we compare this to the MEMS actuation and resonance frequency of a smaller MEMS scanner (20 μm × 20 μm membrane, legs of 20 μm long, 2 μm thick and 2 μm wide), we see that the scan range goes down to 60 nm at 150 V actuation voltage, while the fundamental resonance frequency goes up to 945 kHz. Thus, for scanning very fast on a smooth metal surface,

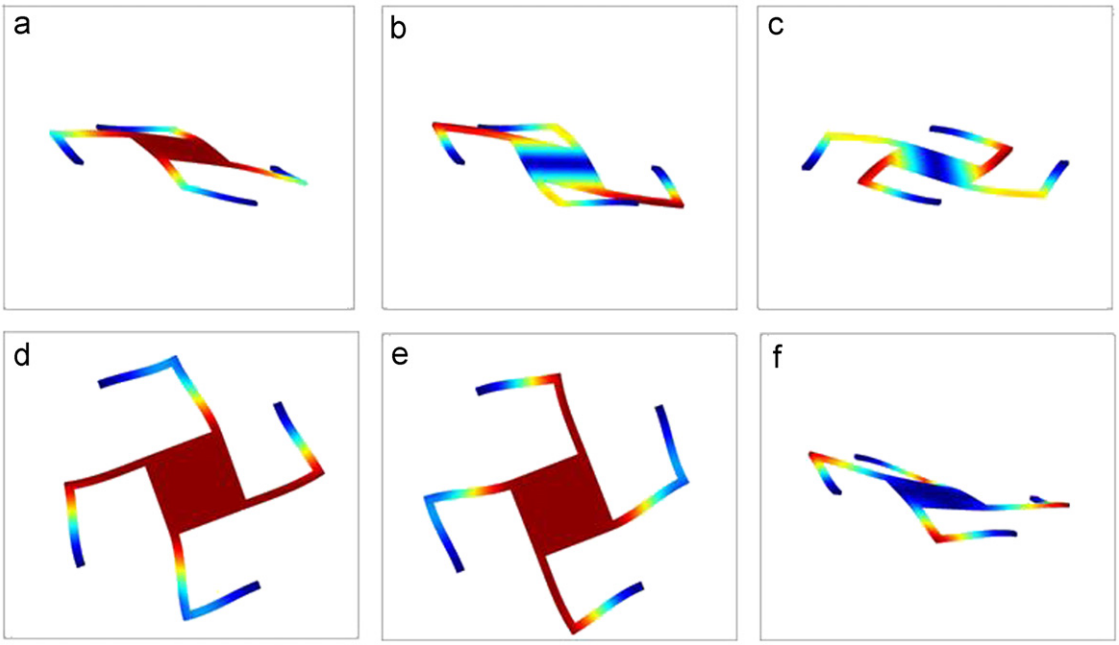

Fig. 5. Dynamic deformation patterns for the first six resonances of a MEMS scanner with a 40×40 μm membrane 40 μm legs with a width of 4 μm. The first resonance is at a frequency of 261 kHz (a), the second (b) and third (c) at approximately 600 kHz, the fourth (d) and fifth (e) are at 921 kHz and the sixth (f) resonance frequency is at 1.1 MHz. The deformations and frequencies have been obtained from finite-element calculations, as explained in the test.

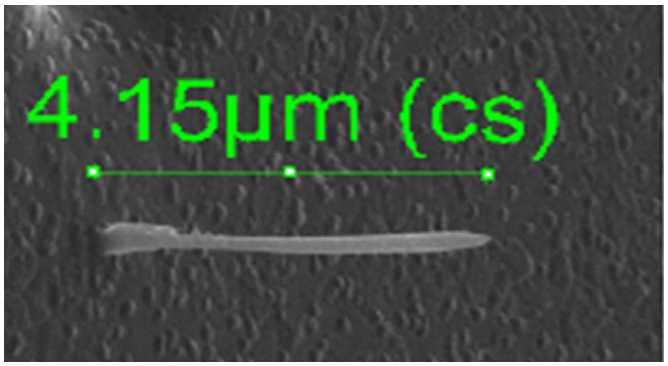

Fig. 6. SEM-image of an EBID-tip as deposited on our MEMS scanner inside a SEM, using $Pt(PF_3)_4$ as a precursor gas. The tip is 4.15 μm long and has an end radius of 20 nm.

the smaller MEMS scanner could be used, whilst scanning samples with a rougher surface would require the larger scanner.

4. Tips

Because we prefer not to use the MEMS scanner as the sample stage (see above), we need to deposit a tip on the MEMS. Attaching a macroscopic tip as is done in a traditional SPM is not an option, since the MEMS are too fragile and since the mass increase would strongly compromise the high resonance frequencies. There are several methods to deposit tips [24,25]. We have used electron beam induced deposition (EBID) of platina from $Pt(PF_3)_4$, that was used as the precursor gas at a pressure of 8×10^{-6} mbar in a 30 kV SEM [26]. This process enables us to grow tips with a length of several micrometers and an end radius of typically 20 nm. A typical result is shown in Fig. 6.

5. Test measurements

To test the functionality of the MEMS SPM scanner, we have integrated it in a DI (Digital Instruments) AFM [27] controlled by LPM (Leiden Probe Microscopy) electronics [28], and in a Nanosurf EasyScan STM [29]. As an illustration of the functionality of the MEMS *z*-scanner, we show here an AFM image of the MEMS scanner surface obtained in an AFM experiment (Fig. 7). The AFM feedback signal was used, after appropriate amplification, to actuate the MEMS scanner, while the *x*,*y*-scanning and the deflection measurement were performed with the DI AFM. It is important to note that in this demonstration experiment the MEMS surface was used as the sample. It was scanned with a regular AFM tip and cantilever while the feedback motion was performed by the membrane. Fig. 7 was obtained with a tip speed of 2 mm/s. Here we see that the peak-to-peak height was 89 nm, while the peak-to-peak deflection was 16 nm. The peak-to-peak deflection indicates to what extent the feedback to the MEMS device has been insufficient to make the AFM tip perfectly follow the surface contour at constant force. The variation in AFM cantilever deflection thus serves as the error signal and in this case the peak-to-peak deflection amounted to 17% of the peak-to-peak height. This ratio is better (i.e. lower) at lower tip speeds. Vertical tip speeds up to 1.2 mm/s and vertical accelerations up to 12 g have been obtained, as calculated from the heightline in Fig. 8. For horizontal tip speeds higher than 2 mm/s, the *xy*-motion excites resonances of the DI AFM (which performs the *xy*-scanning). Therefore, this experiment has not yet tested our MEMS scanners to their limits.

A separate MEMS STM experiment has shown that the conductivity of the EBID-tip is good enough to perform tunneling experiments and also that the native oxide (which is typically present on MEMS structures) does not pose a problem in tunneling experiments. These experiments are described in more detail elsewhere [30].

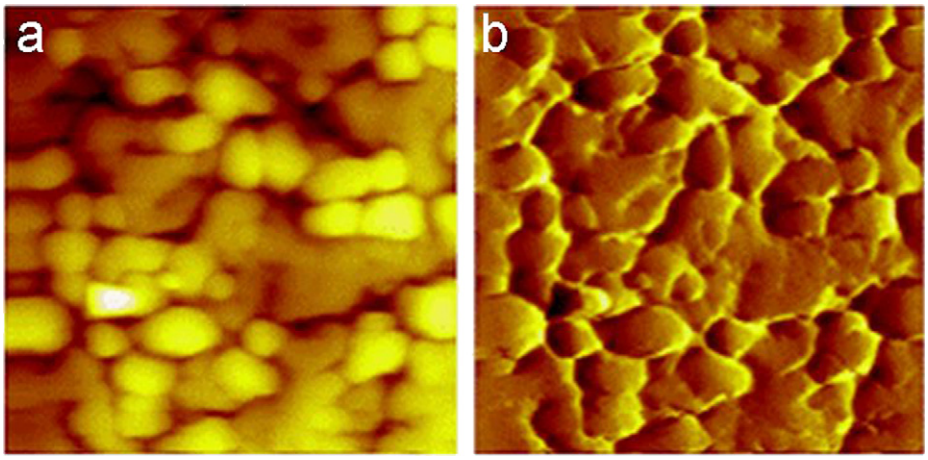

Fig. 7. The MEMS surface scanned in the DI AFM, while the feedback motion was performed by the MEMS itself. (a) Is a topographical image of the surface and (b) is the corresponding deflection image (corresponding to the error signal). The image size is 2 μm × 2 μm. The tip speed was 2 mm/s, corresponding to a frame rate of 1 image/s. The peak-to-peak height is 89 nm and the peak-to-peak deflection is 16 nm. The 'grains' are features of the MEMS SiO_x surface.

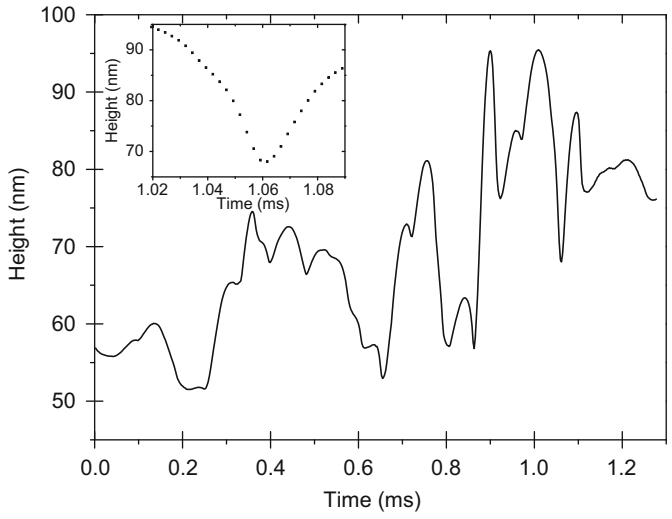

Fig. 8. Heightline from an AFM image with a scan size of 5 μm × 5 μm, obtained with the MEMS *z*-scanner. From this heightline we calculate the vertical acceleration. In the inset a close-up of a steep turn in the height profile is shown; from this data, we calculate the vertical acceleration to be 12 g.

6. Conclusions

We have designed new MEMS SPM scanners that are optimized for high-speed scanning. The most promising geometry was identified as a MEMS *z*-scanner integrated with a macroscopic fast *x*,*y* scan stage. With this combination, we have performed the first fast scan MEMS AFM and STM experiments with our MEMS *z*-scanner. Several hurdles have to be overcome before MEMS scanners can be used routinely as high-quality, fast SPM scanners (as opposed to using them in demonstration experiments). Firstly, the crosstalk between MEMS electrodes, and in STM, the crosstalk between MEMS electrodes and the tunneling current need to be minized. Secondly, an optimum has to be found in the resonance frequency/scan range trade-off. This optimum is different for different applications! On rough surfaces, the *z*-range needs to be higher than on smoother surfaces. Thirdly, sharp tips (i.e. sharper than our EBID-deposited tips) are necessary for imaging with atomic resolution. At this moment, the MEMS scanners are difficult to handle. We are presently standardizing the integration of a MEMS *z*-scanner on a piezo *x*,*y*-scanner.

Acknowledgements

This project was financially supported by a Netherlands SmartMix grant and the NIMIC partner organizations (www.nimic-project.com) through NIMIC, a public-private program. We kindly thank Gert-Jan van Baarle for fruitful discussions.

References

[1] U.B. Arnalds, E.H. Bjarnason, K. Jonsson, S. Olafsson, An externally cooled beetle type scanning tunneling microscope for imaging in cryogenic liquids, Appl. Surf. Sci. 252 (2006) 15.
[2] B.L.M. Hendriksen, S.C. Bobaru, J.W.M. Frenken, Bistability and oscillations in CO oxidation studied with scanning tunnelling microscopy inside a reactor, Catal. Today 105 (2005).
[3] A.J. Katan, T.H. Oosterkamp, Measuring hydrophobic interactions with three-dimensional nanometer resolution, J. Phys. Chem. C 112 (2008).
[4] C.G. Vayenas, S.I. Bebelis, In situ electrochemically controlled promotion of complete and partial oxidation catalysis, Third World Congress on Oxidation Catalysis (1997) 77–92.
[5] M. Kobayashi, K. Sumitomo, K. Torimitsu, Real-time imaging of DNA–streptavidin complex formation in solution using a high-speed atomic force microscope, Ultramicroscopy 107 (2007) 184–190.
[6] H.W. Zandbergen, C.S. Pao, D.J. Srolovitz, Dislocation injection. Reconstruction, and atomic transport on {0 0 1} Au terraces, Phys. Rev. Lett. 98 (2007).
[7] B.Z. Dong, G.J. Fang, J.F. Wang, W.J. Guan, X.Z. Zhao, Effect of thickness on structural, electrical, and optical properties of ZnO: Al films deposited by pulsed laser deposition, J. Appl. Phys. 101 (2007) 3.
[8] T. Fukuma, Y. Okazaki, N. Kodera, T. Uchihashi, T. Ando, High resonance frequency force microscope scanner using inertia balance support, Appl. Phys. Lett. 92 (2008).
[9] M.J. Rost, L. Crama, P. Schakel, E. van Tol, G.B.E.M. van Velzen-Williams, C.F. Overgauw, H. ter Horst, H. Dekker, B. Okhuijsen, M. Seynen, A. Vijftigschild, P. Han, A.J. Katan, K. Schoots, R. Schumm, W. van Loo, T.H. Oosterkamp, J.W.M. Frenken, Scanning probe microscopes go video rate and beyond, Rev. Sci. Instrum. 76 (2005) 053710.
[10] G. Schitter, P.J. Thurner, P.K. Hansma, Design and input-shaping control of a novel scanner for high-speed atomic force microscopy, Mechatronics 18 (2008).
[11] J.H. Kindt, G.E. Fantner, J.A. Cutroni, P.K. Hansma, Rigid design of fast scanning probe microscopes using finite element analysis, Ultramicroscopy 100 (2004).
[12] H. Yamashita, N. Kodera, A. Miyagi, T. Uchihashi, D. Yamamoto, T. Ando, Rev. Sci. Instrum. 78 (2007) 083702.
[13] A.D.L. Humphris, M.J. Miles, J.K. Hobbs, A mechanical microscope: high-speed atomic force microscopy, Appl. Phys. Lett. 86 (3) (2005).
[14] T.R. Albrecht, S. Akamine, M.J. Zdeblick, C.F. Quate, Microfabrication of integrated scanning tunnelling microscope, J. Vac. Sci. Technol. A 8 (1) (1990).
[15] P.F. Indermühle, G. Schürmann, G.A. Racine, N.F. de Rooij, Fabrication and characterization of cantilevers with integrated sharp tips and piezoelectric elements for actuation and detection for parallel AFM applications, Sensors Actuators A 60 (1997).
[16] Y. Xu, N.C. MacDonald, S.A. Miller, Integrated micro-scanning tunneling microscope, Appl. Phys. Lett. 67 (16) (1995).

[17] T. Sulchek, S.C. Minne, J.C. Adams, D.A. Fletcher, A. Atalar, C.F. Quate, Dual integrated actuators for extended range high speed atomic force microscopy, Appl. Phys. Lett. 75 (11) (1999).
[18] P. Vettiger, M. Despont, U. Drechsler, U. Dürig, W. Häberle, M.I. Lutwyche, H. Rothuizen, R. Stutz, R. Widmer, G. Binnig, Millepede: more than one thousand tips for future AFM data storage, IBM J. Res. Develop. 44 (3) (2000) 323–340.
[19] C. Liu, Parallel scanning probe arrays: their applications, Materials Today, 11 (2008).
[20] A. Knoll, P. Bächtold, J. Bonan, G. Cherubini, M. Despont, U. Drechsler, U. Dürig, B. Gotsmann, W. Häberle, C. Hagleitner, D. Jubin, M.A. Lantz, A. Pantazi, H. Pozidis, H. Rothuizen, A. Sebastian, R. Stutz, P. Vettiger, D. Wiesman, E.S. Eleftheriou, Integrating nanotechnology into a working storage device, J. Microelectron. Eng. 83 (2006).
[21] www.memscap.com.
[22] G.M. Rebeiz, in: RF MEMS Theory, Design and Technology, Wiley-Interscience, 2003.
[23] www.comsol.com.
[24] Y. Gan, Atomic and subnanometer resolution in ambient conditions by atomic force microscopy, Surf. Sci. Rep. 64 (2009) 3.
[25] S. Chattopadhyay, L.C. Chen, K.H. Chen, Nanotips: growth, model and applications, Crit. Rev. Solid State Mater. Sci. 31 (2006) 15–53.
[26] A. Botman, M.B.S. Hesselberth, J.J.L. Mulders, Improving the conductivity of platinum-containing nano-structures created by electron-beam-induced deposition, Microelectron. Eng. 85 (2008) 5–6.
[27] www.veeco.com.
[28] www.leidenprobemicroscopy.com.
[29] www.nanosurf.com.
[30] E.C.M. Disseldorp, F.C. Tabak, A.J. Katan, M.B.S. Hesselberth, T.H. Oosterkamp, J.W.M. Frenken, W.M. van Spengen, Challenging SPM speed limits using MEMS technology, Rev. Sci. Instrum., in press.